Transport with reversed shear in the National Spherical Torus Experiment[a)]

F. M. Levinton,[1,b)] H. Yuh,[1] M. G. Bell,[2] R. E. Bell,[2] L. Delgado-Aparicio,[3] M. Finkenthal,[3] E. D. Fredrickson,[2] D. A. Gates,[2] S. M. Kaye,[2] B. P. LeBlanc,[2] R. Maingi,[4] J. E. Menard,[2] D. Mikkelsen,[2] D. Mueller,[2] R. Raman,[5] G. Rewoldt,[2] S. A. Sabbagh,[6] D. Stutman,[3] K. Tritz,[3] and W. Wang[2]
[1]*Nova Photonics, Inc., Princeton, New Jersey 08540*
[2]*Princeton Plasma Physics Laboratory, Princeton, New Jersey 08543*
[3]*Johns Hopkins University, Baltimore, Maryland 21218*
[4]*Oak Ridge National Laboratory, Oak Ridge, Tennessee 37830*
[5]*University of Washington, Seattle, Washington 98195*
[6]*Columbia University, New York, New York 10027*

(Received 3 November 2006; accepted 3 April 2007; published online 16 May 2007)

In the National Spherical Torus Experiment (NSTX) [M. Ono *et al.*, Nucl. Fusion **40**, 557 (2000)], plasmas with strongly reversed magnetic shear, $s \equiv (r/q)(dq/dr) < 0$, in the plasma core exhibit a marked improvement in electron confinement compared to otherwise similar plasmas with positive or only weakly reversed magnetic shear. The q profile itself is determined by the early evolution of the plasma current, the plasma cross section, and the neutral-beam heating power. In the region of shear reversal, the electron thermal diffusivity can be significantly reduced. Detailed experimental investigation of this phenomenon has been made possible by the successful development of a motional Stark effect (MSE) polarimetry diagnostic suitable for the low magnetic field in NSTX, typically 0.35–0.55 T. Measurements of the electron and ion temperature, density, and plasma toroidal rotation profiles are also available with high spatial and temporal resolution for analysis of the plasma transport properties. © *2007 American Institute of Physics*. [DOI: 10.1063/1.2734124]

I. INTRODUCTION

The economic attractiveness of fusion energy could be greatly enhanced by improved transport and stability in fusion devices. Magnetic confinement experiments frequently find cross-field transport to be anomalously high compared to predictions of neoclassical theory, which attributes the energy and particle transport to Coulomb collisions alone. This implies the existence of other sources of transport such as turbulence or stochastic magnetic surfaces. Several experiments have found regimes of transport with improved confinement when there exists in the plasma a region where the magnetic shear, $s \equiv (r/q)dq/dr < 0$. These reversed-shear regimes typically have improved confinement of the ions and frequently, but not always, improvement of the electron thermal diffusivity.[1–5] An understanding of the physics involved in the ion transport reduction has begun to emerge. Several theoretical studies have found that a reduction of the drive for interchange instabilities due to reversed shear can help stabilize or reduce the growth rate of ion temperature gradient (ITG) and trapped electron mode (TEM) microinstabilities.[6–8] Even without completely stabilizing the mode, increased $E_r \times B$ flow shear causes decorrelation of the turbulence, resulting in a reduction of thermal transport,[9,10] particularly the ion transport. Several experimental results and supporting theoretical models have supported this paradigm.[11–15] Despite the complexity of the many contributing and competing effects, including magnetic shear, ion to electron temperature ratio, Shafranov shift, and velocity shear, the computational models have made good progress at predicting suppression of the transport driven by ITG and TEM instabilities. NSTX is predicted[16] to be different from that of conventional aspect ratio tokamaks. With its low aspect ratio, high beta, and low toroidal field, calculations[17] indicate flow shear should facilitate suppression of ion transport. This has been supported by observations that the ion transport is often near neoclassical.[18] NSTX is very suitable for studying electron transport in part because the ions are often near neoclassical and the electron transport is anomalous. Also, NSTX has a comprehensive set of profile diagnostics, necessary for doing transport analysis.

Despite the progress with respect to ion transport, development of an understanding of the electron thermal transport still remains a challenge and continues to be a very active subject of ongoing research, both experimentally and theoretically. An understanding of electron heating and transport is very important because the main heating mechanism in reactor plasmas will be by the α particles which transfer their heat mainly to the electrons. One reason for the difficulty of developing a theoretical understanding of the electron channel is the nonlinear nature and small scale of the electron gyroscale instabilities and the large range of scale lengths needed to address this problem.

Several experiments using predominantly electron heating have observed regimes of improved electron confinement.[19–29] In these experiments it is believed that reversed shear is playing an important role leading to improved electron confinement. However, local magnetic measurements are lacking in most cases to provide definitive data of the q profile evolution. Furthermore, in neutral beam heated

[a)]Paper ZII 3, Bull. Am. Phys. Soc. **51**, 336 (2006).
[b)]Invited speaker.

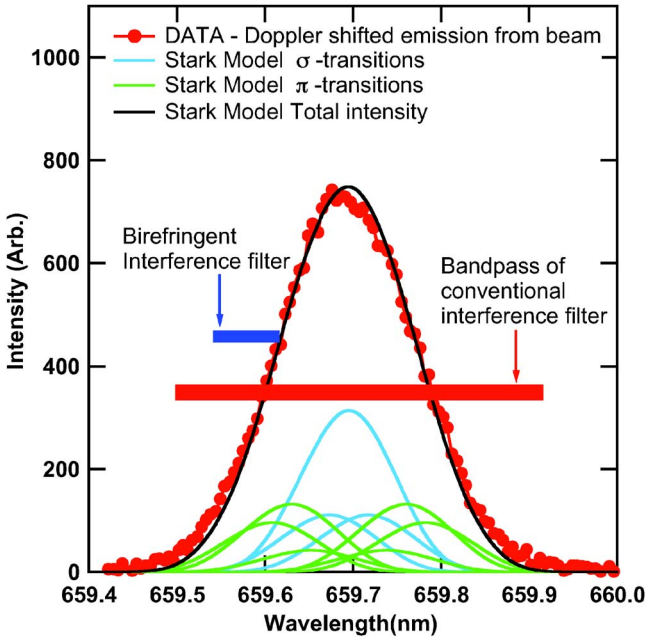

FIG. 1. (Color online) Measured spectrum from the NSTX of Doppler shifter D_α emission from the heating beam. Comparison of the calculated Stark multiplet and its convolution is compared to the measured spectra.

plasmas, the electron thermal diffusivity is often not changed with reversed shear[1,2] and in some cases where it has improved it was affected only over a narrow spatial region near the $q_{\min}$ radius.[30–32] One hypothesis is that the electron temperature gradient (ETG) mode is responsible for the high electron transport routinely observed. The mode has a short wavelength and can exist without affecting the ion transport, consistent with the commonly observed situation in which $\chi_i \ll \chi_e$.

In this paper we report on transport measurements in the low aspect ratio National Spherical Torus Experiment (NSTX),[18,33] where the electron and ion transport, in neutral beam heated discharges, show a clear reduction of the electron thermal diffusivity with reversed shear q profiles and in some cases both the electron and ion thermal diffusivities are reduced.

In Sec. II the motional Stark effect collisional induced fluorescence (MSE-CIF) polarimetry diagnostic, central to this investigation, is briefly described, as it has several unique features due to the low magnetic field of NSTX. The equilibrium reconstruction using the MSE-CIF data is discussed. Section III has a discussion of the formation and evolution of the reversed shear discharge including a case which transitions from reversed shear to one having low central shear (flat q profile) in the plasma core due to a magnetohydrodynamic (MHD) reconnection event. In Sec. IV the transport analysis and results will be described and conclusions are in Sec. V.

II. DIAGNOSTICS

NSTX is a low-aspect-ratio spherical torus. The plasmas used in this study have a low density edge, characteristic of L mode type discharges with about 2 MW of neutral beam

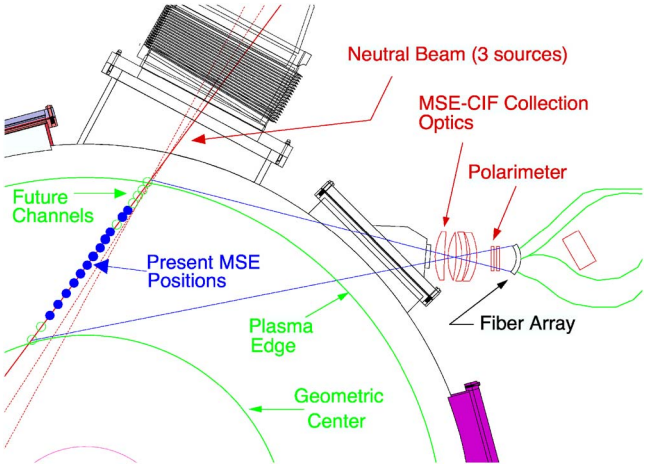

FIG. 2. (Color online) Plan view of MSE-CIF layout on NSTX.

heating. An extensive set of profile diagnostics is used for transport analysis, including ion temperature, ion density, Z-effective, and toroidal flow from the 51-channel charge exchange recombination spectroscopy (CHERS) diagnostic, and electron temperature and density from the 20-channel Thomson scattering. The MHD diagnostics include the Mirnov coils and soft x-ray detector arrays. The measurements of the q profile are made with the 12-channel motional Stark effect polarimetry diagnostic based on collisional induced fluorescence (MSE-CIF).[34] NSTX operates at a toroidal magnetic field of 0.35–0.55 T at the plasma center. This is a significantly lower toroidal magnetic field than for any previous implementation of MSE-CIF polarimetry. In order to obtain a strongly polarized emission signal from the Stark multiplet, a narrow band filter is usually employed to separate out a portion of the spectrum. The spectral splitting of the Stark multiplet of the deuterium Balmer-α line is linearly proportional to the magnetic field, so for the low magnetic field of NSTX the filter bandwidth needs to be reduced substantially. In order to implement the MSE-CIF diagnostic on NSTX, development was required of a new optical filter to achieve higher resolution and throughput than was possible with a conventional interference filter. The filter, based on a wide-field Lyot birefringence interference filter,[35] has achieved a spectral resolution of 0.058 nm. Each filter channel receives light from a bundle of 76 fibers that are 1 mm in diameter. Shown in Fig. 1 is the measured spectrum from NSTX of Doppler shifted D_α emission from collisionally excited neutrals in the heating beam. For comparison is the calculated Stark multiplet and its convolution with the measurement function compared to the measured spectrum. A conventional interference filter with a bandpass of 0.3–0.4 nm would integrate over the entire Stark multiplet of π and σ transitions resulting in a very low polarization fraction, estimated to be $\sim 2\%$. The narrow-band Lyot filter can isolate a portion of the spectrum, such as the π lines, to yield a much higher polarization fraction, measured to be 40%. With the good polarization fraction using the Lyot filter and large étendue of the optical system, the resulting time resolution is 5–10 ms with a statistical uncertainty of $\leq 0.2°$ for the measured magnetic field pitch angle. A plan view of

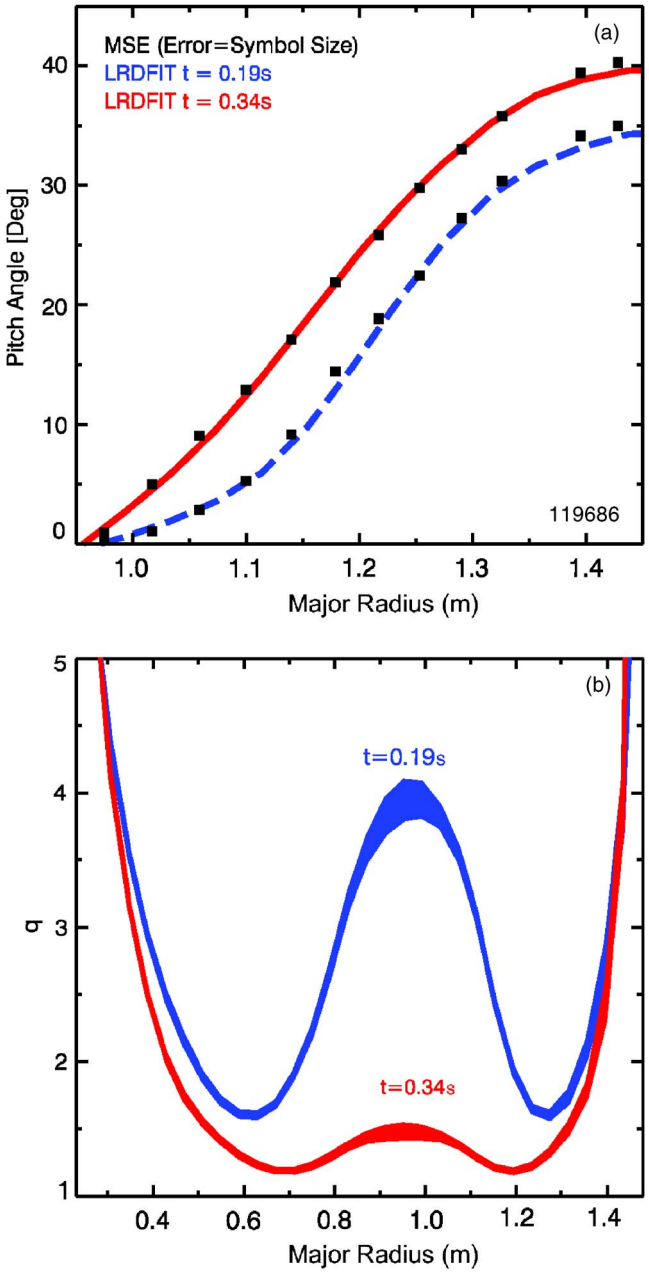

FIG. 3. (Color online) MSE-CIF data and reconstruction results from LRDFIT at two times. (a) Pitch angle at $t=0.19$ s (dashed line) and $t=0.34$ s (solid line) and (b) the corresponding q profiles. The bands on the q profile represents the variability from LRDFIT.

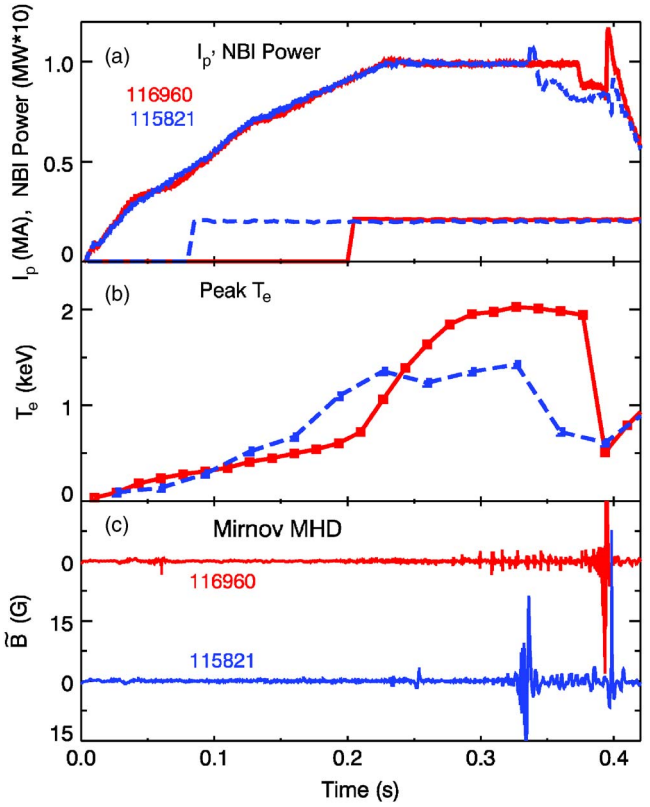

FIG. 4. (Color online) (a) The plasma current, neutral beam power, (b) peak electron temperature, and (c) Mirnov coil signals for two discharges. The solid line corresponds to the discharge with reversed shear (116960) and dashed line (115821) with a low central shear q profile.

the MSE-CIF diagnostic on the NSTX is shown in Fig. 2. The filter is tuned to select the emission from just one of the neutral beam sources which have different Doppler shifts due to the different injection angles. There is no interference from the other neutral beam sources, so MSE measurements are not constrained. The MSE-CIF system presently has 12 sight lines operating out of a possible 19, covering from the magnetic axis to the outboard edge, with a spatial resolution of 2–3 cm.

The magnetic field pitch angle from the MSE-CIF diagnostic, along with the external coil currents, magnetic field coils, and flux loop measurements are input into the free boundary LRDFIT equilibrium reconstruction code. LRDFIT includes a circuit model of the eddy currents in the vacuum vessel that has been validated by experiments. The reconstruction includes a T_e isosurface constraint and toroidal rotation effects. The MSE-CIF data is affected by intrinsic radial electric fields in the plasma.[36] The data are corrected for the radial electric field, E_r, due to the measured toroidal rotation and pressure gradients terms in the radial force balance shown in Eq. (1) using the CHERS data. E_r is given by the radial force balance equation,

$$E_r = \frac{1}{n_i Z_i e} \nabla P_i - v_{\theta i} B_\phi + v_{\phi i} B_\theta \tag{1}$$

where P_i is the ion pressure, n_i is the ion number density, $Z_i e$ is the ion charge, $v_{\theta i}(v_{\phi i})$ is the poloidal (toroidal) velocity, and $B_\theta(B_\phi)$ is the poloidal (toroidal) magnetic field. The E_r correction does not yet include effects from poloidal flow, which are expected to be quite small based on neoclassical theory estimates from NCLASS.[37] The poloidal flow calculated from the NCLASS code is less them 10 km/s across the plasma profile. Poloidal velocity measurements are available for the plasma edge region only, where values of $\leq$10 km/s have been measured.[38] Based on a poloidal flow of 10 km/s the effect on the MSE data would amount to less than a 1% correction. Shown in Fig. 3 is a reconstruction from LRDFIT of two cases of the pitch angle profile compared to the input MSE-CIF data. The MSE-CIF error bars are shown in the plot by the size of the symbol. The reconstruction from LRDFIT has low residuals of ~0.3° in the

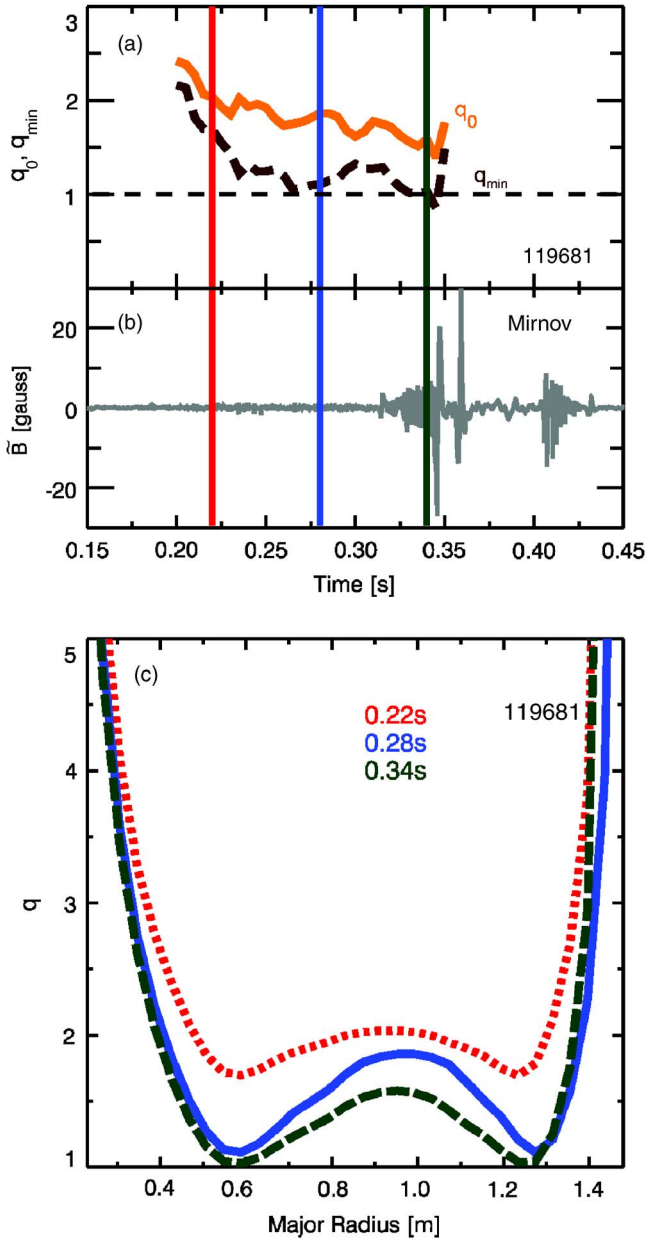

FIG. 5. (Color online) A reversed shear discharge evolution of (a) $q(0)$ (solid line), q_{min} (dashed line), and (b) Mirnov coil data. (c) The q profiles at 0.22 s (dotted line), 0.28 s (solid line), and 0.34 s (dashed line) are also indicated by vertical lines in (a) and (b).

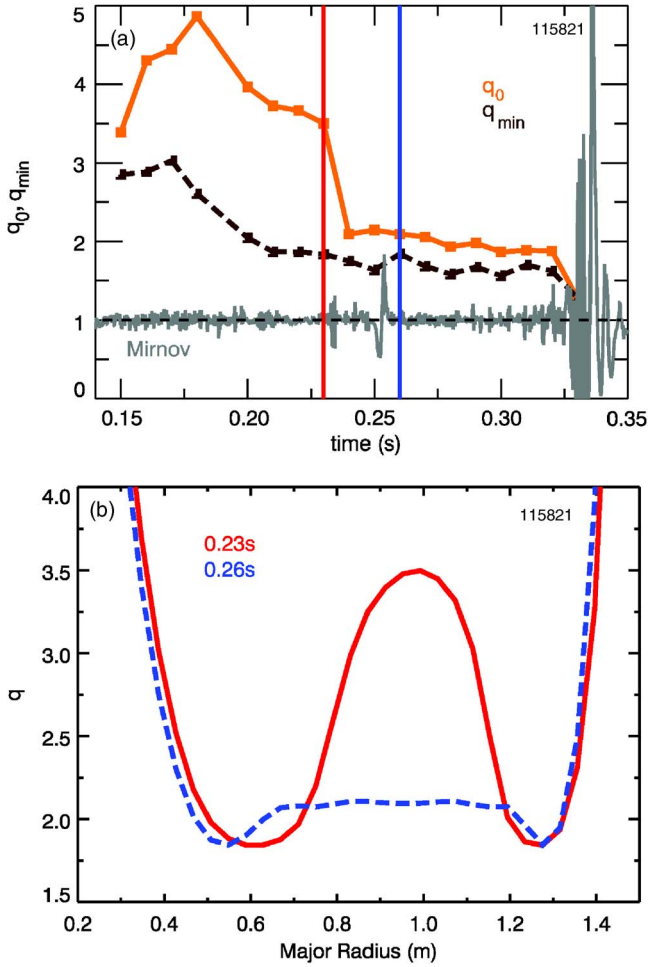

FIG. 6. (Color online) The (a) $q(0)$ (solid line) and q_{min} (dashed line) evolution. At 0.235 s $q(0)$ drops precipitously following a MHD event. (b) The q profiles just before (solid line) and after (dashed line) the MHD event at 0.235 s.

plasma core, consistent with the MSE-CIF uncertainties. The magnetic axis, corresponding to the pitch angle going through 0°, is at $R=0.96$ m and $R=0.97$ m for the two times shown. The bands on the q profile represents the variability from LRDFIT. The very good fit is indicative of the self consistency of the MSE-CIF data combined with the Thomson scattering and external magnetics data used as constraints in the equilibrium reconstruction code. If the data were not self-consistent the fits and residuals would be quite large. The bands on the reconstructed q profiles from LRDFIT represent the variation of the q profile by varying the input parameters to LRDFIT.

III. q PROFILE DEVELOPMENT AND EVOLUTION

We have several controls available to vary the startup and evolution of the current density profile in NSTX. Such variables as the plasma growth and shape, plasma current ramp rate, neutral beam timing, and gas fueling have all been found to have a strong effect on the current profile evolution. The basic reversed shear development scenario is to create a large plasma as early as possible during the current ramp up phase. In this way the resistive diffusion of the current from the edge is slowed down forming a hollow current profile. In order to slow the current penetration to the plasma core and maintain the hollow current profile, early neutral beam heating is applied to heat the electrons and thereby increase the conductivity. We have found that without careful control of the various parameters such as the current ramp rate and neutral beam timing, MHD instability can occur that causes reconnection and a very rapid current redistribution. However, with the MSE-CIF diagnostic to monitor the effects of MHD activity, the plasma evolution can be optimized to produce the desired results. Figure 4 shows the waveforms for the current ramp-up, neutral beam timing, and the peak electron temperature for two cases, having the same growth and

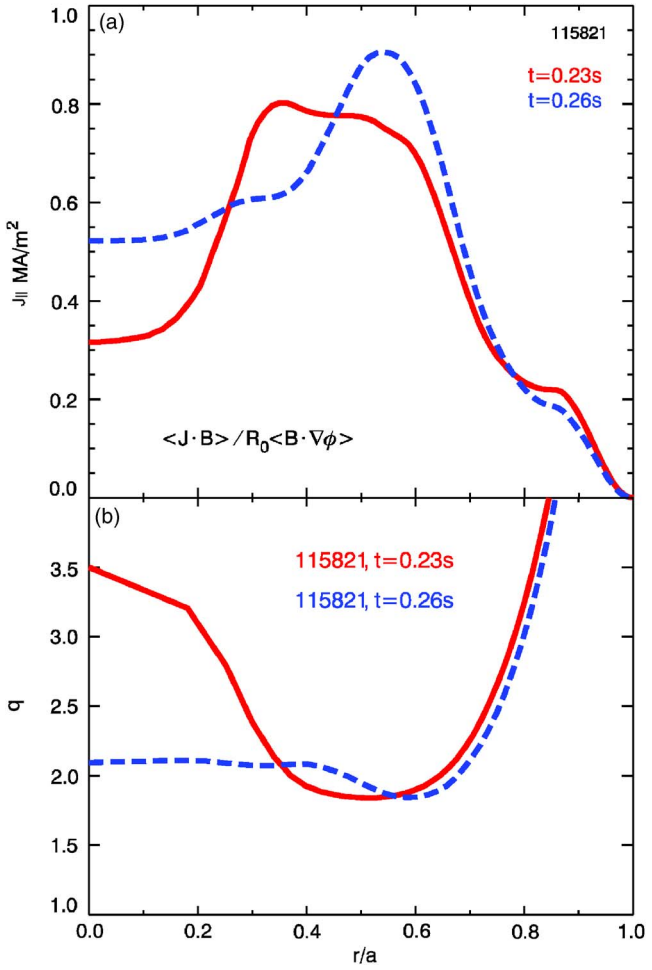

FIG. 7. (Color online) (a) Parallel current density profile and (b) $q(r/a)$ before (solid line) and after (dashed line) reconnection at 0.235 s.

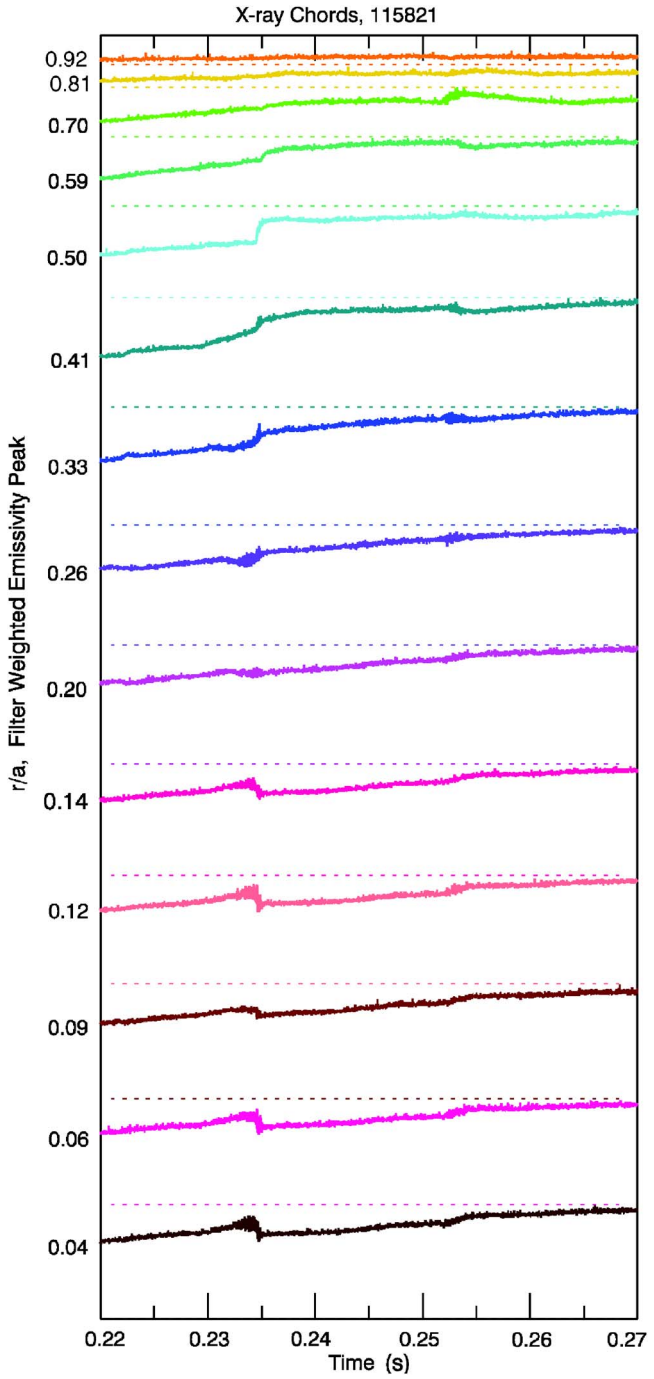

FIG. 8. (Color online) Soft x-ray data with sawtooth-like MHD event at 0.235 s.

current ramp up, but different timing for the start of neutral beam injection. The later start time is our reversed shear scenario. Shown in Fig. 5 are the $q(0)$, $q_{\min}$, MHD evolution, and q profiles for this case. One neutral beam source, with 2 MW of injected power, is turned on at 0.2 s, just before $q(0)$ and $q_{\min}$ decrease below 2. Only one source is used to minimize the MHD present during the discharge. Both $q(0)$ and $q_{\min}$ decrease as the current slowly penetrates to the plasma center. As $q_{\min}$ approaches 1, the MHD activity begins to grow, and when $q_{\min}$ reaches 1, the mode locks and the plasma collapses. Prior to that the MHD signal is very quiescent.

The case with the earlier start of neutral beam injection begins with a high $q(0)$ that is strongly reversed, but the plasma undergoes a MHD-triggered reconnection at $t=0.235$ s that flattens the q profile producing a substantial region of low magnetic shear. The time evolution of $q(0)$, $q_{\min}$, and the MHD activity indicated by the Mirnov coil are shown in Fig. 6. Prior to a small MHD event at 0.235 s, $q(0)=3.5$. The next time slice, at $t=0.24$, has $q(0)\sim 2$, with little change in $q_{\min}$. The MSE-CIF q profiles, in Fig. 6, show a large difference before and after the MHD reconnection occurs. After the reconnection event, the q profile is flat inside of $q=2$. Large changes such as this are not predicted by the classical or neoclassical field diffusion model, and this emphasizes the need for local measurements of the magnetic field pitch angle profile to correctly determine the current density evolution. The parallel current density profile, shown in Fig. 7, is calculated from the LRDFIT equilibrium reconstruction code. It is interesting to compare this to the soft x-ray array diagnostic, shown in Fig. 8. The x-ray data has been mapped, using the equilibrium from LRDFIT, to the minor radius. The radii of the x-ray chords correspond to the location of the peak calculated emission, based on mapping the electron density, electron temperature, and Z-effective to

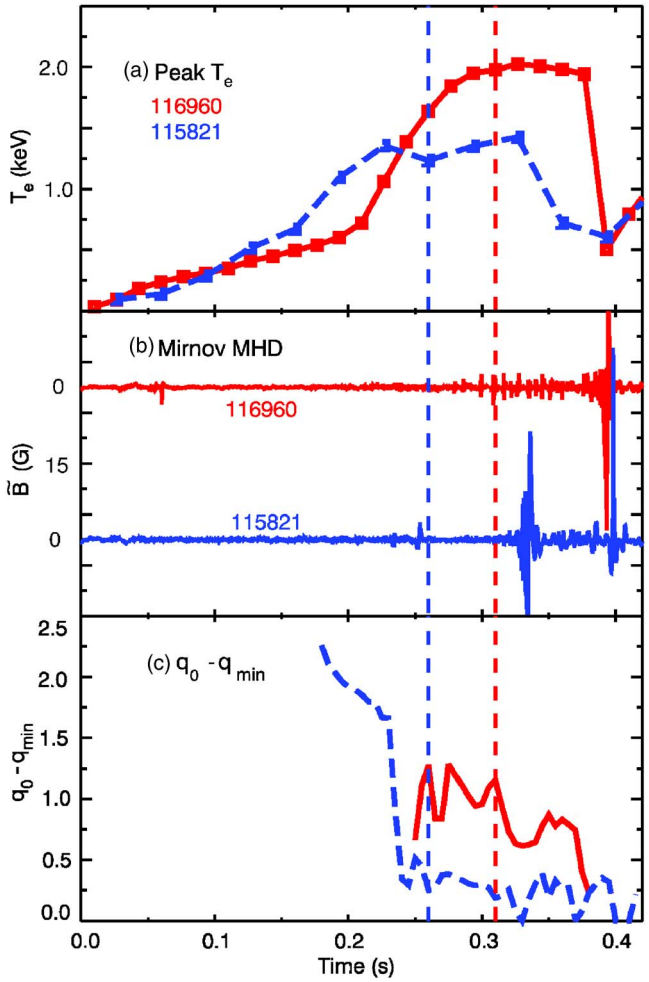

FIG. 9. (Color online) Comparison of (a) peak electron temperature evolution, (b) Mirnov coil data, and (c) $q(0)-q_{\min}$ evolution for reversed shear discharge (solid line) and low shear discharge (dashed line).

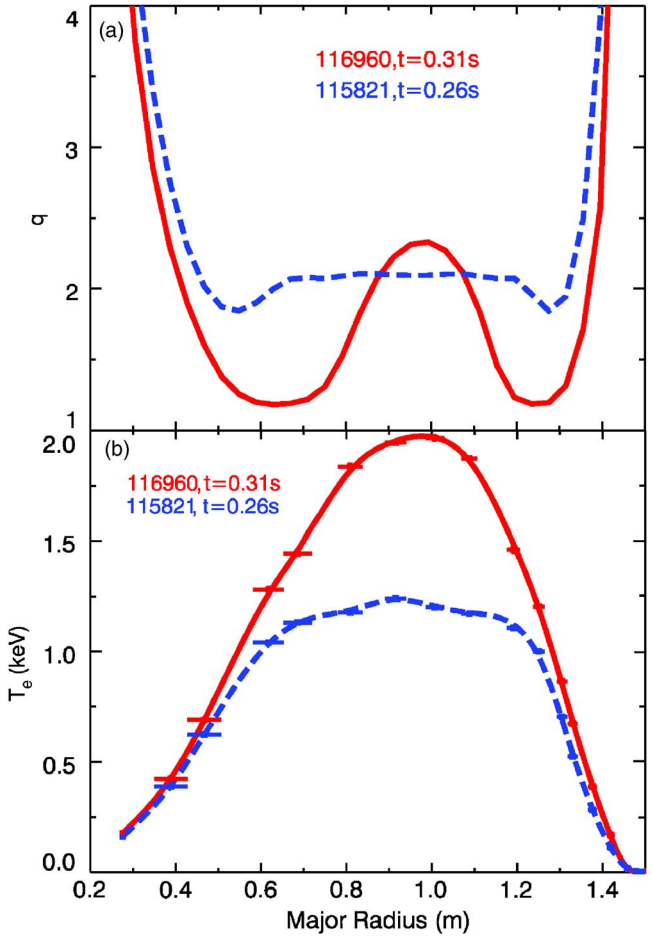

FIG. 10. (Color online) The (a) q profiles and (b) electron temperature profiles at times shown at 0.31 (solid line) and 0.26 (dashed line).

the flux surfaces and calculating the local intensity. The x-ray data show a sawtooth-like event at 0.235 s. The location where the parallel current density profiles cross, near $r/a \sim 0.25$, correspond closely to the inversion radius of the x-ray data. Also, the outboard edge of the x-ray data extends to the location of the $q_{\min}$ radius, that is shown in Fig. 7.

IV. TRANSPORT ANALYSIS

The local transport analysis involves the TRANSP code[39] using all the available kinetic profile data and the equilibrium from the LRDFIT reconstruction that is constrained by the MSE-CIF data. To evaluate the effect of the q profile and in particular the local magnetic shear, on the transport, we shall compare two cases: (i) two discharges, one that remained with a reversed shear q profile and another that did not; (ii) a discharge that transitions from a reversed shear q profile to a low central shear q profile. In case (i) the peak electron temperature, Mirnov coil data, and $q(0)-q_{\min}$ evolution are shown in Fig. 9 and the q profiles and electron temperature profiles in Fig. 10. Neither discharge indicated in Fig. 9 has any appreciable MHD activity at the time of interest or for some duration before. The reversed shear discharge has a much more peaked electron temperature profile shown in Fig. 10. The location at which the two temperature profiles begin to strongly diverge, at 1.25 m, corresponds to the $q_{\min}$ radius. Outboard of the $q_{\min}$ radius the temperature profiles are very similar. This is also much the same for the density profiles. The ion temperature profile shows a similar behavior for the two cases, as shown in Fig. 11. However, the toroidal velocity profiles show little difference. The corresponding electron and ion thermal diffusivities for these two discharges are shown in Fig. 12. Representative error bars for the uncertainties of the thermal diffusivities is shown in the figure based on an analysis for similar discharges.[40] The relative uncertainty is approximately constant across the profile. The reversed discharge has a lower electron thermal diffusivity by almost an order of magnitude compared to the discharge with low central shear. The diffusivity profiles diverge strongly inside of $r/a \sim 0.4$, which corresponds to the region of the reversed shear as shown in Fig. 13. The ion transport also shows some improvement in the plasma core, however the estimated neoclassical value as calculated by NCLASS (Ref. 37) also decreases. The ion thermal diffusivity remains near the neoclassical level in the plasma core for both cases.

As described earlier, some discharges make a transition from reversed shear to low central shear over a very short time interval. The evolution of $q(0)$, $q_{\min}$, MHD, and the q

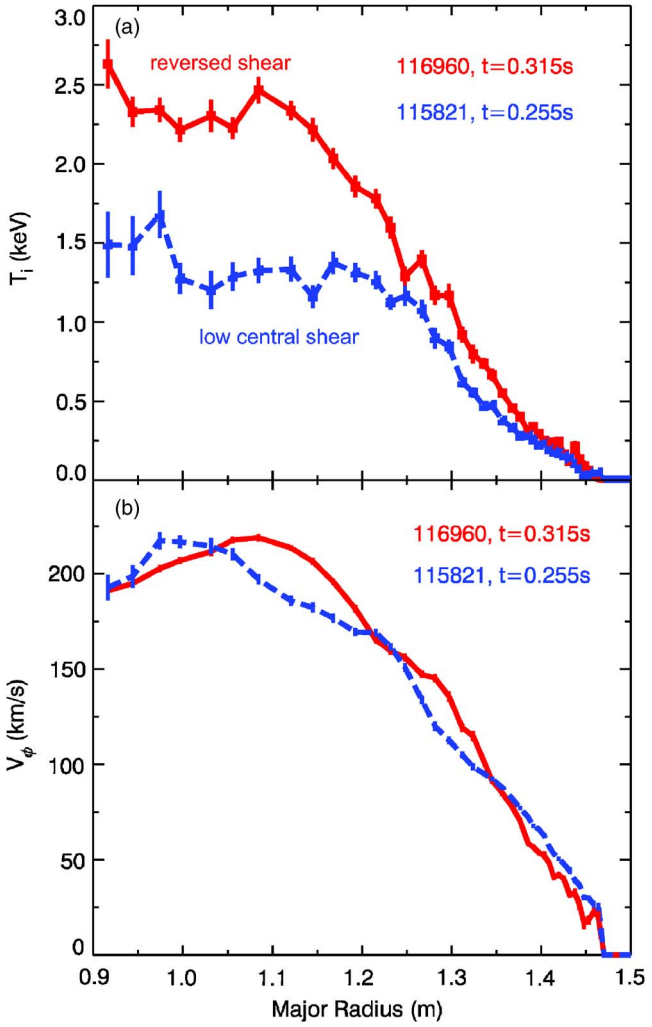

FIG. 11. (Color online) The (a) ion temperature and (b) toroidal rotation velocities at 0.315 s for the reversed shear discharge (solid lines) and 0.255 s for the low central shear discharge (dashed line).

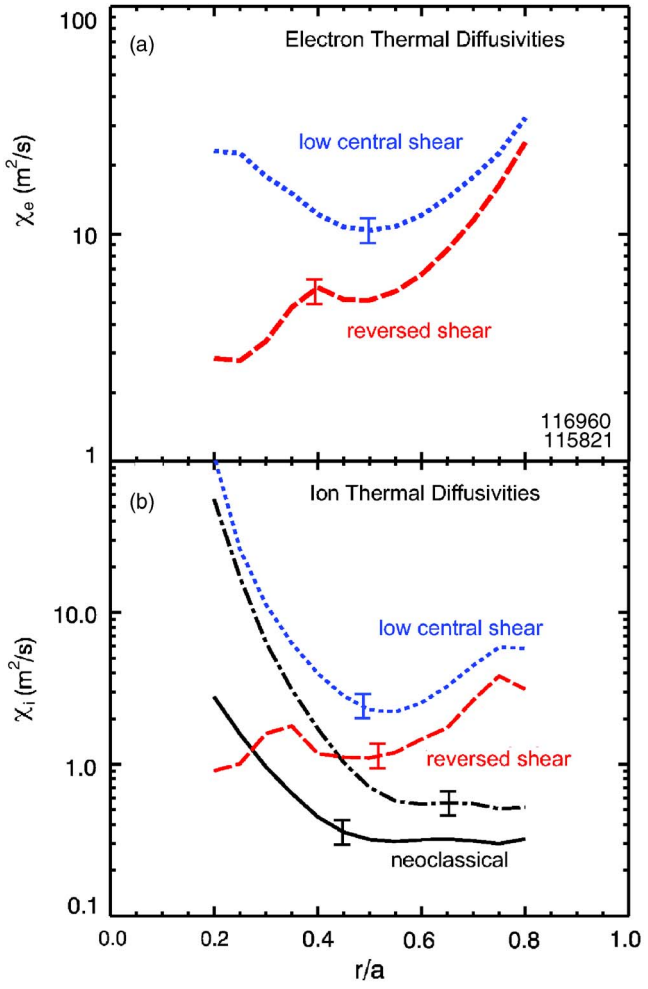

FIG. 12. (Color online) The (a) electron thermal diffusivity for the low central shear (dotted line) and reversed shear (dashed line) cases. (b) Comparison of ion thermal diffusivity of the reversed shear (dashed line), low central shear (dotted line), and neoclassical calculations for low central shear (dashed-dotted line) and reversed shear (solid line).

profile change are shown in Figs. 6 and 7. The electron thermal diffusivity also increases just after the reversed shear profile changes to low central shear, as shown in Fig. 14. Like the previous case the change in χ_e is almost an order of magnitude and the sharp change in the χ_e profiles occurs inboard of the $q_{\min}$ radius. Unlike the previous case, however, the χ_i profiles do not change significantly, as shown in Fig. 14, but neither does the neoclassical level. In this case also both the reversed shear and low central shear χ_i profiles are near or slightly above the calculated neoclassical level in the plasma core.

Analysis of these profiles has been done with the GYRO,[41] GTC,[42] and GS2 (Ref. 43) microstability codes. The nonlinear GYRO simulations predicts finite growth rates from ITG/TEM modes with $k_\theta \rho_i < 1$. However these modes are fully quenched by flow shear across the entire plasma for both the reversed shear and low shear profiles. These results are also consistent with calculations done with the GTC code for ITG modes. This does not explain the higher ion thermal diffusivity in the outer half of the plasma which is well above the neoclassical predicted level. A natural candidate for the electron transport would be the shorter wavelength

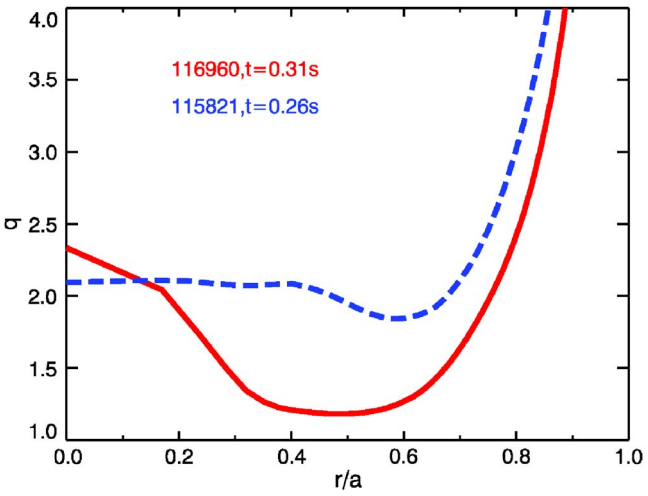

FIG. 13. (Color online) $q(r/a)$ for the reversed shear (solid line) and low central shear (dashed line) discharges.

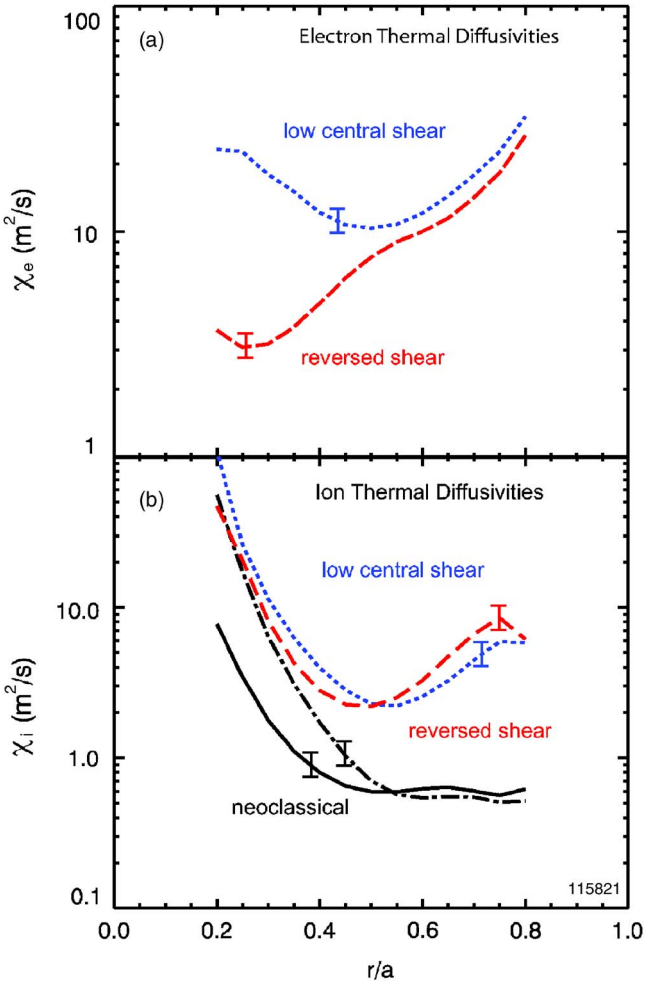

FIG. 14. (Color online) The (a) electron thermal diffusivity for the low central shear (dotted line) and reversed shear (dashed line) of the same discharge at different times. (b) Comparison of ion thermal diffusivity of the reversed shear (dashed line), low central shear (dotted line), and neoclassical calculations for low central shear (dashed-dot line) and reversed shear (solid line).

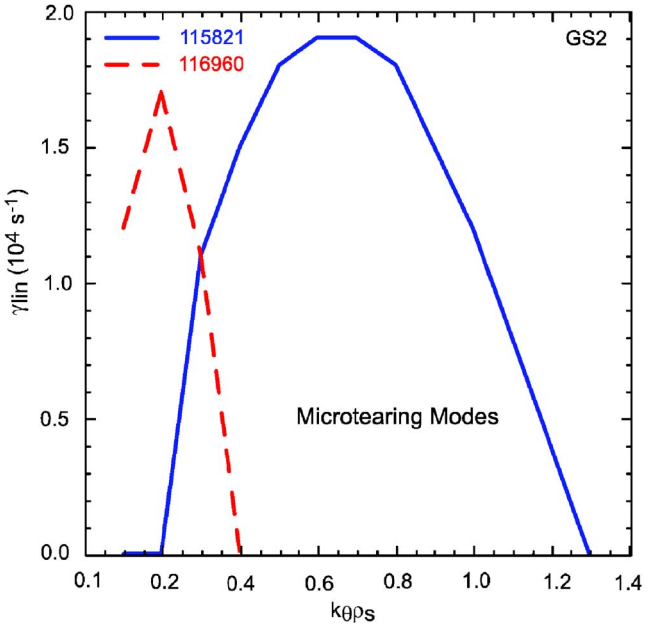

FIG. 15. (Color online) The microtearing mode growth rates for the reversed shear case (116960 dashed line) and low shear condition (115821 solid line) at $r/a=0.3$.

electron temperature gradient (ETG) turbulence[44] or microtearing modes. For the electron channel, with $k_\theta \rho_i > 10$, ETG modes are calculated with the GS2 code to be linearly stable in both discharges. However, this is not the case for microtearing modes from the GS2 code simulations. These modes are calculated to be unstable at $r/a=0.3$ for both the low shear and reversed shear discharges. However, as shown in Fig. 15 the reversed shear case has a smaller region at lower k_θ that is unstable compared to the low shear case which has a large region in k_θ space that is unstable. This is consistent with our experimental results that shows lower electron thermal diffusivity with reversed shear. Previous transport analysis, without q profile measurements, for NSTX (Ref. 45) also concluded that microtearing modes are a likely cause of the large electron thermal diffusivity observed. The microtearing modes preferentially drives electron transport, but can also drive ion energy transport. This may play a role in the higher than neoclassical ion thermal diffusivity that is observed in the region $r/a > 0.5$. Further nonlinear microtearing calculations will be needed to quantitatively compare the numerical models to the observed electron and ion thermal diffusivity profiles.

V. CONCLUSIONS

We have reported results of experiments whose goal was to generate various q profiles with differing magnetic shear, as determined by detailed measurements with the MSE-CIF diagnostic, in order to study the effect of the q profile on plasma transport. Several cases were produced and analyzed, ranging from strongly reversed to low magnetic shear. The correlation between reversed magnetic shear and reduced electron transport in NSTX has been clearly shown and that weak shear is not sufficient to cause this decrease in transport. This would rule out the zero-shear gap (ZSG) model[46] which attempts to explain the reduction of transport by an increase in the distance between resonant surfaces in the region of low shear. If this were the case one would expect the flat q profile in Fig. 6 to have the better transport, but in fact it does not. Our results are also not consistent with models that depend on rational q surfaces and are independent of shear.[28] Several experiments have observed the improvement only over a narrow region at the $q_{\min}$ radius. However, we also see the improvement in χ_e over the region from the $q_{\min}$ radius to the magnetic axis. In the regime in which we are operating on NSTX, the ion thermal transport is at or near the neoclassical level in the plasma core. This is consistent with calculations of ITG/TEM microinstabilities which indicate that with flow shear they are fully stabilized in the plasma core. Electron energy transport is well above the neoclassical level, however, it is significantly improved with reversed shear q profiles. The electrons are linearly stable to ETG modes, but unstable to microtearing modes. The microtearing modes with the low shear q profile have a wider range of k_θ that are unstable and present a possible explana-

tion to the observed improvement in electron transport with reversed shear. Further nonlinear microtearing calculations will be needed to quantitatively understand the measured electron transport observed in the NSTX.

ACKNOWLEDGMENTS

This research is supported by U.S. DOE Grant No. DE-FG02-99ER54520 and U.S. DOE Contract No. DE-AC02-76CH03073.

[1] F. M. Levinton, M. C. Zarnstorff, S. H. Batha *et al.*, Phys. Rev. Lett. **75**, 4417 (1995).
[2] E. J. Strait, L. L. Lao, M. E. Mauel *et al.*, Phys. Rev. Lett. **75**, 4421 (1995).
[3] O. Gruber, R. C. Wolf, R. Dux *et al.*, Phys. Rev. Lett. **83**, 1787 (1999).
[4] S. Ishida, T. Fujita, H. Akasaka, N. Akino, K. Annou, and T. Aoyagi, Phys. Rev. Lett. **79**, 3917 (1997).
[5] C. Gormezano, Y. F. Baranov, C. D. Challis, I. Coffey, G. A. Cottrell, A. C. Ekedahl, and C. M. Greenfield, Phys. Rev. Lett. **80**, 5544 (1998).
[6] J. F. Drake, Y. T. Lau, P. N. Guzdar, A. B. Hassam, S. V. Novakovski, and A. Zeiler, Phys. Rev. Lett. **77**, 494 (1996).
[7] R. E. Waltz, G. D. Kerbel, J. Milovich, and G. W. Hammett, Phys. Plasmas **2**, 2408 (1995).
[8] M. A. Beer, G. W. Hammett, G. Rewoldt, E. J. Synakowski, and M. C. Zarnstorff, Phys. Plasmas **4**, 1792 (1997).
[9] F. L. Hinton and G. M. Staebler, Phys. Fluids B **5**, 1281 (1993).
[10] G. M. Staebler, F. L. Hinton, J. C. Wiley, R. R. Dominguez, C. M. Greenfield, P. Gohil, T. K. Kurki-Suonio, and T. H. Osborne, Phys. Plasmas **1**, 909 (1994).
[11] K. H. Burrell, Phys. Plasmas **4**, 1499 (1997).
[12] E. J. Synakowski, S. H. Batha, M. A. Beer *et al.*, Phys. Rev. Lett. **78**, 2972 (1997).
[13] C. Gormezano, Plasma Phys. Controlled Fusion **41**, B367 (1999).
[14] Y. Kamada, Plasma Phys. Controlled Fusion **42**, A65 (2000).
[15] P. W. Terry, Rev. Mod. Phys. **72**, 109 (2000).
[16] G. Rewoldt, W. M. Tang, S. Kaye, and J. Menard, Phys. Plasmas **3**, 1667 (1996).
[17] M. Kotschenreuther, W. Dorland, Q. P. Liu, M. C. Zarnstorff, R. L. Miller, and Y. R. LinLiu, Nucl. Fusion **40**, 677 (2000).
[18] M. Ono, S. M. Kaye, Y. K. Peng, G. Barnes, W. Blanchard, and M. D. Carter, Nucl. Fusion **40**, 557 (2000).
[19] X. Litaudon, Y. Peysson, T. Aniel *et al.*, Plasma Phys. Controlled Fusion **43**, 677 (2001).
[20] E. Barbato, Plasma Phys. Controlled Fusion **43**, A287 (2001).
[21] P. Buratti, E. Barbato, G. Bracco, S. Cirant, F. Crisanti, and G. Granucci, Phys. Rev. Lett. **82**, 560 (1999).
[22] N. C. Hawkes, Y. Andrew, C. D. Challis, R. DeAngelis, V. Drozdov, J. Hobirk, and E. Joffrin, Plasma Phys. Controlled Fusion **44**, 1105 (2002).
[23] N. A. Kirneva, Y. V. Esipchuk, A. A. Borschegovskij, V. V. Chistyakov, E. P. Gorbunov, and V. P. Denisov, Plasma Phys. Controlled Fusion **47**, 1787 (2005).
[24] C. Gormezano, A. Becoulet, P. Buratti, L. Carraro, F. Crisanti, and B. Esposito, Plasma Phys. Controlled Fusion **46**, B435 (2004).
[25] Y. F. Baranov, X. Garbet, N. C. Hawkes, B. Alper, R. Barnsley, and C. D. Challis, Plasma Phys. Controlled Fusion **46**, 1181 (2004).
[26] T. Fujita, T. Fukuda, Y. Sakamoto, S. Ide, T. Suzuki, and H. Takenaga, Plasma Phys. Controlled Fusion **46**, A35 (2004).
[27] K. A. Razumova, V. V. Alikaev, A. A. Borschegovskii, V. V. Chistyakov, M. M. Dremin, and A. V. Gorshkov, Nucl. Fusion **42**, 973 (2000).
[28] G. M. D. Hogeweij, N. J. L. Cardozo, M. R. D. Baar, and A. M. R. Schilham, Nucl. Fusion **38**, 1881 (1998).
[29] M. A. Henderson, Y. Camenen, S. Coda, T. P. Goodman, P. Nikkola, A. Pochelon, O. Sauter, and the TCV Team, Phys. Rev. Lett. **93**, 215001 (2004).
[30] B. W. Stallard, C. M. Greenfield, G. M. Staebler, C. L. Rettig, M. S. Chu, M. E. Austin, D. R. Baker, and L. R. Baylor, Phys. Plasmas **6**, 1978 (1999).
[31] T. Fujita, S. Ide, H. Shirai, M. Kikuchi, O. Naito, and Y. Koide, Phys. Rev. Lett. **78**, 2377 (1997).
[32] M. G. Bell, R. E. Bell, P. C. Efthimion, D. R. Ernst, E. D. Fredrickson, and F. M. Levinton, Plasma Phys. Controlled Fusion **41**, A719 (1999).
[33] S. M. Kaye, M. G. Bell, R. E. Bell, S. Bernabei, J. Bialek, T. Biewer, and W. Blanchard, Nucl. Fusion **45**, S168 (2005).
[34] F. M. Levinton, R. J. Fonck, G. M. Gammel, R. Kaita, H. W. Kugel, E. T. Powell, and D. W. Roberts, Phys. Rev. Lett. **63**, 2060 (1989).
[35] A. M. Title and W. J. Rosenberg, Opt. Eng. **20**, 815 (1981).
[36] M. C. Zarnstorff, F. M. Levinton, S. H. Batha, and E. J. Synakowski, Phys. Plasmas **4**, 1097 (1997).
[37] W. Houlberg, K. C. Shaing, S. P. Hirshman, and M. C. Zarnstorff, Phys. Plasmas **4**, 3230 (1997).
[38] T. M. Biewer, R. E. Bell, S. J. Diem, C. K. Phillips, J. R. Wilson, and P. M. Ryan, Phys. Plasmas **12**, 056108 (2005).
[39] R. J. Hawryluk, in *Physics of Plasmas Close to Thermonuclear Conditions*, Varenna 1979, edited by B. Coppi, G. G. Leotta, D. Pfirsch, R. Pozzoli, and E. Sindoni (Commission of the European Communities, Brussels, 1981), Vol. 1, p. 19.
[40] B. P. LeBlanc, R. E. Bell, S. M. Kaye *et al.*, Nucl. Fusion **44**, 513 (2004).
[41] R. E. Waltz, J. M. Candy, and M. N. Rosenbluth, Phys. Plasmas **9**, 1938 (2002).
[42] W. X. Wang, Z. Lin, W. M. Tang, W. W. Lee, S. Ethier, J. L. V. Lewandowski, G. Rewoldt, T. S. Hahm, and J. Manickam, Phys. Plasmas **13**, 092505 (2006).
[43] M. Kotschenreuther, G. Rewoldt, and W. M. Tang, Comput. Phys. Commun. **88**, 128 (1995).
[44] W. Horton, B. G. Hong, and W. M. Tang, Phys. Fluids **31**, 2971 (1988).
[45] D. Stutman, M. Finkenthal, K. Tritz, M. H. Redi, S. M. Kaye, M. G. Bell, and B. P. LeBlanc, Phys. Plasmas **13**, 092511 (2006).
[46] Y. Kishimoto, J. Y. Kim, W. Horton, T. Tajima, M. J. LeBrun, S. A. Dettrick, J. Q. Li, and S. Shirai, Nucl. Fusion **40**, 667 (2000).